Structural Chemistry
https://doi.org/10.1007/s11224-022-01908-0

ORIGINAL RESEARCH

Synthesis of the nickel(II) complexes bearing tetradentate thiosemicarbazone through Michael addition of n-alcohols. Experimental, theoretical characterization and antioxidant properties

Tuncay Karakurt[1] · Büşra Kaya[2] · Onur Şahin[3] · Bahri Ülküseven[2]

Received: 27 October 2021 / Accepted: 3 March 2022

Abstract
New thiosemicarbazone derivative, 3-benzylidene-2,4-pentanedione-S-methyl-thiosemicarbazone hydrogen iodide (TSC), was synthesized and characterized by elemental analysis, IR, ^{1}H NMR and single crystal X-ray diffraction. The novel nickel(II) complexes, Ni1-4, were synthesized from the TSC and salicylaldehyde by template effect of nickel(II) ion. The reactions were accomplished by a proton provided from the addition of alcohols which are methyl, ethyl, propyl and allyl for complexes Ni1, 2, 3 and 4, respectively. Spectroscopic data indicated that the formation of the complexes occurred through Michael addition of the alcohols to the 2,4-pentanedione moiety of the TSC. Distorted square planar structures of complexes Ni1 and Ni2 were confirmed by single crystal X-ray diffraction. In addition, the detailed computations were performed by using the theory DFT for experimentally obtained structures of the TSC, Ni1 and Ni2. The antioxidant property of the TSC and nickel(II) complexes along with the standard ascorbic acid was studied by using DPPH radical scavenging and Cupric Reducing Antioxidant Capacity (CUPRAC) assays.

Keywords Thiosemicarbazone · Nickel(II) complexes · Micheal addition · DFT · Antioxidant activity

Introduction

Thiosemicarbazones are known as a class of compounds exhibiting beneficial biological activity and are the subject of many studies [1]. Triapine that is being tested clinically against cancer cells and Dp44mT, which has been studied intensively due to its selective antitumor and antimetastatic properties, are some of the candidates promising drug ingredients [2, 3]. Other examples, methisazone, thioacetone, and ambazon, are anti-infective thiosemicarbazone derivatives [4–6]. It has been observed that an increase in activity is provided for thiosemicarbazones by forming complexes with metal ions [7–10].

✉ Büşra Kaya
busra.kaya@istanbul.edu.tr

[1] Department of Chemical and Process Engineering, Faculty of Engineering-Architecture, Kırsehir Ahi Evran University, 40100 Kırsehir, Turkey

[2] Department of Chemistry, Faculty of Engineering, Istanbul University-Cerrahpasa, 34320 Istanbul, Turkey

[3] Department of Occupational Health & Safety, Faculty of Health Sciences, Sinop University, TR-57000 Sinop, Turkey

Transition metal complexes of tetradentate thiosemicarbazones were reported to have important pharmacological properties [11–13]. The complexes with salen-like N_2O_2 donor thiosemicarbazones have shown significant biological activities such as cytotoxic activity in various cancer cell lines [14, 15], DNA binding and cleavage [16, 17] and enzyme inhibition [18]. In a study, it was shown that an N_2O_2-type nickel(II)-thiosemicarbazone complex can induce HL60 leukemia cells apoptosis by inhibiting the PI3K/Akt pathway [19].

Reactive oxygen species (ROS) and free radicals such as superoxide anion, hydrogen peroxide, and hydroxyl radical can cause oxidative stress that reasons serious damage in lipids, proteins, and the DNA of bio-tissues [20]. Therefore, it is substantial to improve compounds with high antioxidant activity to prohibit the formation of ROS and free radicals. In recent years, radical scavenging activity of some copper(II)-thiosemicarbazone complexes has drawn great interest [21, 22]. In addition, the antioxidant properties of some iron(III), mangan(III) nickel(II), and oxovanadium(IV) complexes with N_2O_2-thiosemicarbazones have been reported [23–25].

Published online: 21 March 2022

There are a few reports on the synthesis of palladium(II)-thiosemicarbazone complexes via Michael addition [1, 26]. These studies include Michael addition of methyl alcohol. Herein, we present the novel nickel(II) complexes obtained through Michael addition of methyl, ethyl, propyl, and allyl alcohols (Fig. 1). The TSC and nickel(II) complexes were characterized by analytical and spectroscopic methods. Additionally, structures of TSC, Ni1, and Ni2 have been authenticated by single crystal XRD analysis and supported by theoretical calculations. The antioxidant potential of the compounds was screened in the scavenging activity of DPPH• and cupric ions (Cu^{2+}) reducing power (CUPRAC).

Experimental

Materials and methods

Elemental analyses were carried out using a Thermo Finnigan Flash EA 1112 analyzer. FT-IR spectra were obtained using an Agilent Carry 630 FT-IR spectrometer in ATR mode. NMR spectrum was recorded in $CDCl_3$/DMSO-d_6 solvent on a Varian UNITY INOVA 500 MHz spectrometer. Magnetic measurements were carried out at room temperature by the Gouy technique with a MK I model device obtained from Sherwood Scientific.

For X-Ray diffraction analysis, suitable crystals were selected and data collection was performed on a Bruker diffractometer equipped with a graphite-monochromatic Mo-K_α radiation at 296 K. The structures were solved by direct methods using SHELXS-2013 [27] and refined by full-matrix least-squares methods on F^2 using SHELXL-2013 [28] from within the WINGX [29] suite of software. All non-hydrogen atoms were refined with anisotropic parameters. The hydrogen atoms of nitrogen atoms in TSC were found from the electron density-difference map; they were refined with individual isotropic displacement parameters. All other hydrogen atoms were placed in ideal calculated positions and refined as riding atoms with relative isotropic displacement parameters. Bruker APEX2 [30] was used for data collection, while molecular diagrams were created using MERCURY [31].

Molecular modeling for TSC molecule, Ni1 and Ni2 complexes was carried out with the Gaussian 09 program [32] using the basic functional density theory DFT/B3LYP [33, 34] with LanL2DZ [35–37] bas set. Optimized structures of the compounds were obtained with the Gaussian 09 program (Figure S2). The IR spectra, frontier orbitals and molecular electrostatic potential (MEP) map calculations were made using the optimized structures of the TSC, Ni1, and Ni2.

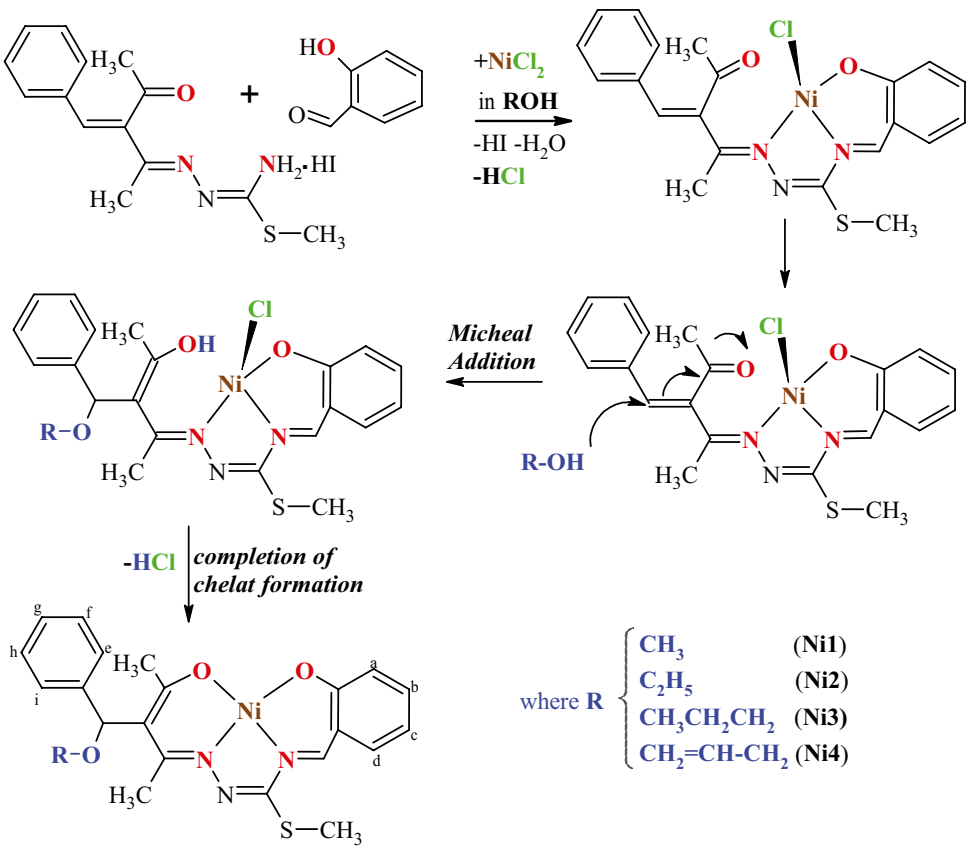

Fig. 1 Possible formation mechanism for the nickel(II) complexes

Synthesis

3-benzylidene-2,4-pentanedione-S-methyl-thiosemicarbazone hydrogen iodide (TSC)

The TSC was synthesized from the reaction between 3-benzylidene-2,4-pentanedione (1.7 mL, 10 mmol) and S-methylthiosemicarbazone hydrogen iodide (2.33 g, 10 mmol) in methyl alcohol [38]. The mixture was stirred at room temperature for 2 h. Upon cooling the solution in refrigerator at 4 °C, a light yellow precipitate was formed. The solid was filtered, washed with methanol and dried in vacuo. The crystals suitable for X-ray diffraction were obtained from slow evaporation of the methyl alcohol-dichloromethane (2:1) solution.

Yield: 2.62 g, 65%. Mp: 160 °C. Anal. Calcd for $C_{14}H_{17}N_3OS.HI$ (%): C, 41.70; H, 4.50; N, 10.42; S, 7.95. Found: C, 41.56; H, 4.34; N, 10.31; S, 7.76. FT-IR (υ, cm^{-1}): 3246, 3164 (NH_2), 3043 ($CH_{aromatic}$) 1694 (C = O), 1627–1588 (C = N, C = C). ^{1}H NMR (δ, ppm): 8.62 (s, 2H, NH_2), 7.45 – 7.35 (m, 6H, *aromatic*), 2.63 (s, 3H, SCH_3), 2.45 (s, 3H, CCH_3), 2.29 (s, 3H, CCH_3).

Nickel(II) complexes (Ni1-4)

A methanolic (5 mL) solution of $NiCl_2.6H_2O$ (0.24 g, 1 mmol) was added to the mixture of TSC (0.4 g, 1 mmol) and salicylaldehyde (0.1 mL, 1 mmol) in methyl alcohol (5 mL) [39, 40]. The light brown color solution was stirred for 5 min and Et_3N (0.2 mL) was then added. After standing for 4 h at room temperature, the red-colored complex was isolated by filtration, washed with methanol and hexane, and dried in vacuo. The red crystals of Ni1 suitable for X-ray diffraction were obtained by recrystallization from methyl alcohol-dichloromethane (1:3) solution. Synthesis of Ni2 was performed by using ethyl alcohol instead of methyl alcohol. The red-colored complex was recrystallized from ethyl alcohol-dichloromethane (1:3) mixture to gain crystals suitable for X-ray diffraction. In synthesis of Ni3 and Ni4, propyl and allyl alcohols were used as solvents, respectively.

Ni1. Yield: 0.14 g, 28%. Mp: 238 °C. μ_{eff}: 0.035 BM. Anal. Calcd for $C_{22}H_{23}N_3NiO_3S$ (%): C, 56.44; H, 4.95; N, 8.97; S, 6.85. Found: C, 56.28; H, 4.81; N, 8.74; S, 7.36. FT-IR (υ, cm^{-1}): 1612, 1582, 1553 (C = N^1, C = N^2, N^4 = C), 2918, 2812 (C-H), 1165 (C–O–C), 1145, 1128 (C-O). ^{1}H NMR (δ, ppm): 7.89 (s, 1H, N = C*H*), 7.29 – 7.21 (m, 5H, *e-i*), 7.16 (d, 1H, *d*), 6.92 (d, 1H, *a*), 6.73 (d, 1H, *c*), 6.58 (t, 1H, *b*), 5.51 (s, 1H, = C*H*), 3.35 (s, 3H, OCH_3), 2.55 (s, 3H, SCH_3), 2.27 (s, 3H, CCH_3), 2.19 (s, 3H, CCH_3).

Ni2. Yield: 0.11 g, 23%. Mp: 197 °C. μ_{eff}: 0.042 BM. Anal. Calcd for $C_{23}H_{25}N_3NiO_3S$ (%): C, 57.29; H, 5.23; N, 8.71; S, 6.65. Found: C, 57.60; H, 4.94; N, 8.47; S, 7.06. FT-IR (υ, cm^{-1}): 1611, 1580, 1550 (C = N^1, C = N^2, N^4 = C), 2967, 2921 (C-H), 1164 (C–O–C), 1144, 1129 (C-O). ^{1}H NMR (δ, ppm): 7.93 (s, 1H, N = C*H*), 7.89 (d, 2H, *c,d*), 7.72 – 7.33 (m, 5H, *e-i*), 7.21 (d, 1H, *a*), 6.73 (t, 1H, *b*), 5.27 (s, 1H, = C*H*), 3.75–3.71 (m, 2H, OCH_2), 2.62 (s, 3H, SCH_3), 2.35 (s, 3H, CCH_3), 2.19 (s, 3H, CCH_3), 1.26 (t, 3H, CCH_3).

Ni3. Yield: 0.10 g, 20%. Mp: 171 °C. μ_{eff}: 0.020 BM. Anal. Calcd for $C_{24}H_{27}N_3NiO_3S$ (%): C, 58.09; H, 5.48; N, 8.47; S, 6.46. Found: C, 57.84; H, 5.29; N, 8.19; S, 6.92. FT-IR (υ, cm^{-1}): 1610, 1578, 1552 (C = N^1, C = N^2, N^4 = C), 2958, 2921 (C-H), 1163 (C–O–C), 1144, 1126 (C-O). ^{1}H NMR (δ, ppm): 7.94 (s, 1H, N = C*H*), 7.90 (d, 2H, *c,d*), 7.67 – 7.39 (m, 5H, *e-i*), 7.22 (d, 1H, *a*), 6.74 (t, 1H, *b*), 5.28 (s, 1H, = C*H*), 3.64 (t, 2H, OCH_2), 2.67 (s, 3H, SCH_3), 2.35 (s, 3H, CCH_3), 2.20 (s, 3H, CCH_3), 1.64–1.57 (m, 2H, CCH_2C), 0.96 (t, 3H, CCH_3).

Ni4. Yield: 0.07 g, 14%. Mp: 207 °C. μ_{eff}: 0.012 BM. Anal. Calcd for $C_{24}H_{25}N_3NiO_3S$ (%): C, 58.32; H, 5.10; N, 8.50; S, 6.49. Found: C, 58.05; H, 4.87; N, 8.33; S, 6.88. FT-IR (υ, cm^{-1}): 1610, 1579, 1553 (C = N^1, C = N^2, N^4 = C), 3020, 3005 (C = CH_2), 1164 (C–O–C), 1145, 1127 (C-O). ^{1}H NMR (δ, ppm): 7.85 (s, 1H, N = C*H*), 7.81 (d, 2H, *c,d*), 7.57 – 7.29 (m, 5H, *e-i*), 7.15 (d, 1H, *a*), 6.62 (t, 1H, *b*), 5.95–5.92 (m, 1H, = CH), 5.24 (d, 1H, = CH_aH), 5.19 (s, 1H, = C*H*), 5.10 (d, 1H, = C*H*H_b), 4.10 (d, 2H, OCH_2), 2.57 (s, 3H, SCH_3), 2.34 (s, 3H, CCH_3), 2.11 (s, 3H, CCH_3).

Antioxidant tests

CUPRAC assay

Antioxidant capacity was determined by using the CUPRAC method. Molar absorption (Ɛ) coefficients were calculated for each compound with linear calibration curve. For determination, to a test tube were added in the order of 1 mL of 10 mM $CuCl_2.2H_2O$, 1 mL of 7.5 mM Nc, 1 mL of 1.0 M pH 7 NH_4Ac buffer solution, x mL antioxidant sample solution, and (1.1-x) mL H_2O. The mixture was incubated for 30 min, and the absorbance was measured at 450 nm [41]. The TEAC coefficients (trolox equivalent antioxidant capacities) were calculated as the ratio of the molar absorptivity of each compound to that from the trolox method ($Ɛ_{trolox}$: 1.67×10^4 L mol^{-1} cm^{-1}).

DPPH radical scavenging assay

The radical scavenging activity of the compounds was tested with reference to DPPH (2,2-diphenyl-1-picrylhydrazyl) radicals. Firstly, the percentages of radical scavenging activity were found using the absorbance values, and then their corresponding IC_{50} values were calculated. The measurements were carried out at different concentrations (5, 10, 15, 20, and 25 μM). The solution of the test material was mixed

with 2-mL DPPH (100 μM) and final volume made up to 4 ml using methanol [42]. After mixing gently, the mixture was incubated in dark for 30 min and the absorbance was measured at 515 nm. All determinations were performed in triplicate. The percentage of scavenging activity was determined by the following equation:

$$\text{DPPH radical scavenging activity (\%)} = [(A_{control} - A_{sample})/A_{control}] \times 100.$$

where $A_{control}$ = absorbance of control and A_{sample} = absorbance of sample solution at 515 nm. % scavenging percentages were plotted against the different concentrations, and IC_{50} values were calculated from the graph.

Results and discussion

Synthesis and spectral elucidation

The new thiosemicarbazone, TSC, was synthesized by the reaction of 3-benzylidene-2,4-pentanedione with the equivalent amount of S-methylthiosemicarbazone hydrogen iodide in methyl alcohol. The product was obtained as a light yellow solid in good yield (65%). Novel nickel(II) complexes, Ni1-4, were formed by adding one equivalent of nickel chloride to a mixture of the TSC and salicylaldehyde at room temperature, as indicated in Fig. 1. The diamagnetic complexes were obtained in relatively low yields as red-colored solids. They were air stable, soluble in chlorinated hydrocarbons and polar solvents, and insoluble in hydrocarbons and water.

The formation of the nickel(II) complexes can be considered in four stages:

(1) Nickel ion performs a template reaction between thioamide nitrogen (N^4) and salicylaldehyde, leading to the simultaneous coordination of imine nitrogen (N^1) and phenolic oxygen.
(2) The Michael addition of alcohols (methyl, ethyl, propyl or allyl alcohol) to the C = C bond in 2,4-pentanedione moiety.
(3) An enol-tautomer formation in the moiety through the additional H atom.
(4) Separation of HCl, coordination of the deprotonated oxygen to the nickel center, thus completing the complex formation [1].

In brief, the proton gained from the addition of alcohol provided the 6.5,6-membered chelate system and so the complex formation. Our experiments showed that the addition of the alcohols does not occur in the absence of nickel(II). For this reason, nickel ions are thought to play a role also in the Michael addition in addition to the template effect.

IR spectrum of the TSC showed two bands in the 3246 and 3164 cm^{-1} resulting from the NH_2 stretchings. The C = O and C = C, C = N stretching bands were identified at 1694 and 1627–1588 cm^{-1} region, respectively. On complexation, there was a disappearance of NH_2 and C = O bands and decrease in the imine (1612–1610 cm^{-1}) stretching frequencies. The new bands corresponding to N^4 = C vibrations around 1550 cm^{-1}, indicating the condensation reaction between CH = O of salicylaldehyde and NH_2 of thioamide. Furthermore, the observation of υ(C-H) bands in the range of 3020–2812 cm^{-1} and υ(C–O–C) bands around 1160 cm^{-1} were evidence that the complex formation realized through the Michael addition of the alcohols.

After obtaining the stable structures of TSC, Ni1, and Ni2 by DFT/B3LYP/LanL2DZ model, we simulated their IR spectra with same model to compare with experimental data. We multiply the calculated frequency values with a scaling factor of 0.961. The C = O, NH_2 and C = C, C = N stretching bands of the TSC molecule were calculated at 1612, 3367–3545, and 1506–1582 cm^{-1} region, respectively. The N^4 = C vibrations, υ(C-H) and υ(C–O–C) bands of the Ni1 complex were calculated at 1557–1500, 3101–3033, and 1030 cm^{-1}, respectively, while for the Ni2 complex they were calculated at 1558–1501, 3166–3097, and 1039 cm^{-1}.

The ^{1}H NMR spectrum of the TSC mainly exhibited three sets of signals. First, the NH_2 protons were observed at 8.62 ppm as a singlet. In the spectra of the complexes, this signal disappeared as expected. The second set of signals corresponding to the aromatic protons due to the benzyl group were observed around 7.45–7.35 ppm in the spectrum of the TSC, whereas they were seen around 7.90–6.58 ppm as combined with salicylaldehyde protons in the complex spectra. The HI proton did not appear in the spectrum, probably because it is highly dissociated. The last set of signals appeared at 2.63, 2.45, and 2.29 ppm corresponded to SCH_3 and CCH_3 protons, respectively. For the complexes, resonances of the aliphatic protons due to CCH_3 and SCH_3 groups were in the same range that of the TSC. Besides, the new signals appeared at 7.94–7.85 and 5.51–5.19 ppm in the spectra of the complexes were assigned to the N^4 = CH and C = CH protons, respectively, which confirmed the chelate formation around nickel(II).

A new signal appeared at 3.35 ppm in the spectrum of the Ni1 was assigned to the OCH_3 protons. The ethoxy protons, OCH_2 and CH_3, of the Ni2 were observed in the region 3.75–3.71 and 1.26 ppm, respectively. In the spectrum of Ni3, OCH_2 and CH_3 protons were recorded at 3.64 and 0.96 ppm as triplets, whereas CH_2 protons 1.64–1.57 ppm as a multiplet. The characteristic peak pattern at around 5.95, 5.24 and 4.10 ppm clearly showed the presence of the allyloxy group in the Ni4 spectrum (Fig. 2). The presence of these signals in the spectra of complexes confirmed that the Michael addition of the alcohols had occurred during the complex formation.

Description of the crystal structures

The molecular structures of TSC, Ni1, and Ni2 with the atom numbering schemes are shown in Fig. 3. Compound TSC crystallize in the space group *C2/c*, while compounds Ni1 and Ni2 crystallize in the space group *P-1* (Table 1). The asymmetric unit of Ni2 contains two crystallographically independent molecules (Z ' = 2) with similar parameters but different conformation, while the asymmetric units of TSC and Ni1 contain one molecule. The thiosemicarbazone ligand has N_2O_2 donor set. Nickel(II) ion in Ni1 is coordinated by two nitrogen [Ni1-N1 = 1.836(3) Å, Ni1-N3 = 1.828(3) Å] and two oxygen atoms [Ni1-O1 = 1.848(3) Å, Ni1-O2 = 1.826(3) Å]. The equivalent bond lengths of Ni2 are between 1.819(5) and 1.833(6) Å for Ni–N and 1.822(4) and 1.847(4) Å for Ni–O (Table S1). The nickel(II) centers have distorted square planar coordination geometries. In TSC, the combination of N–H···I hydrogen bonds produces $C_2^2(4)$ chain (Fig. S1a) which is running parallel to the [010] direction (Table S2). In Ni1, the combination of C-H···O hydrogen bonds (Table S2) generating 2D supramolecular network (Fig. S1b). The molecules of Ni2 are connected by C-H···π interactions (Table S2). The combination of C-H···π interactions produces edge-fused $R_2^2(12)R_2^2(22)$ rings (Fig. S1c) running parallel to the [111] direction.

Electronic properties and MEP maps

In the theoretical calculations, the fractional coordinates obtained from the X − ray diffraction data were used as the initial geometry. Optimized structures of the TSC, Ni1, and Ni2 were given in Figure S2. Frontier orbitals (FMOs) are the most important orbitals in molecules, they consist of the highest occupied molecular orbital (HOMO) with electron donating groups and the lowest unoccupied molecular orbital (LUMO) with electron acceptor groups [43, 44]. Also, the energy gap between these two orbitals helps to describe the chemical reactivity, ionization potential, kinetic stability, chemical hardness, and softness of the molecule [45–47]. The distributions and energy levels of FMOs for the compounds are shown in Fig. 4. The calculated energy between the HOMO and LUMO gap is 2.64 eV for TSC while the calculated energy gaps of the Ni1 and Ni2 complexes are 3.08 and 3.07 eV, respectively.

The atomic contribution of the 5 highest atoms to these orbitals; LUMO: N30(16%) + C14(13%) + N33(11%) + C6(7%) + C1(6%), HOMO: C25(%28) + S32(%14) + C20(%10) + N33(%10) + N35(%5) for TSC, LUMO: C9(21%) + N7(9%) + N6(8%) + C26(8%) + C12(6%), HOMO: C16(%18) + N5(%14) + Ni(%11) + S2(%10) + O4(%10) for Ni1, and LUMO: C11(20%) + N50(9%) + N49(8%) + C4(7%) + C1(6

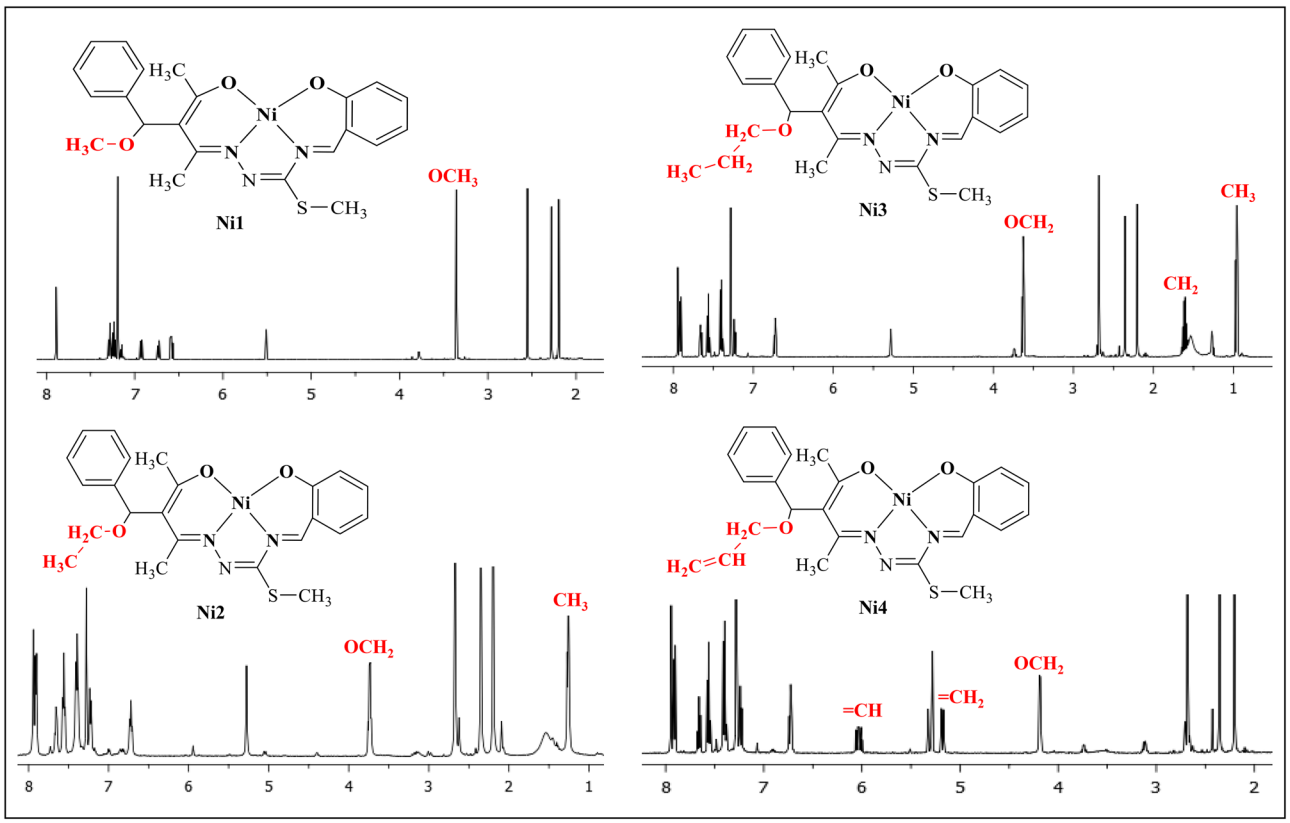

Fig. 2 ^{1}H NMR spectra of the nickel(II) complexes (Ni1-4) in $CDCl_3$

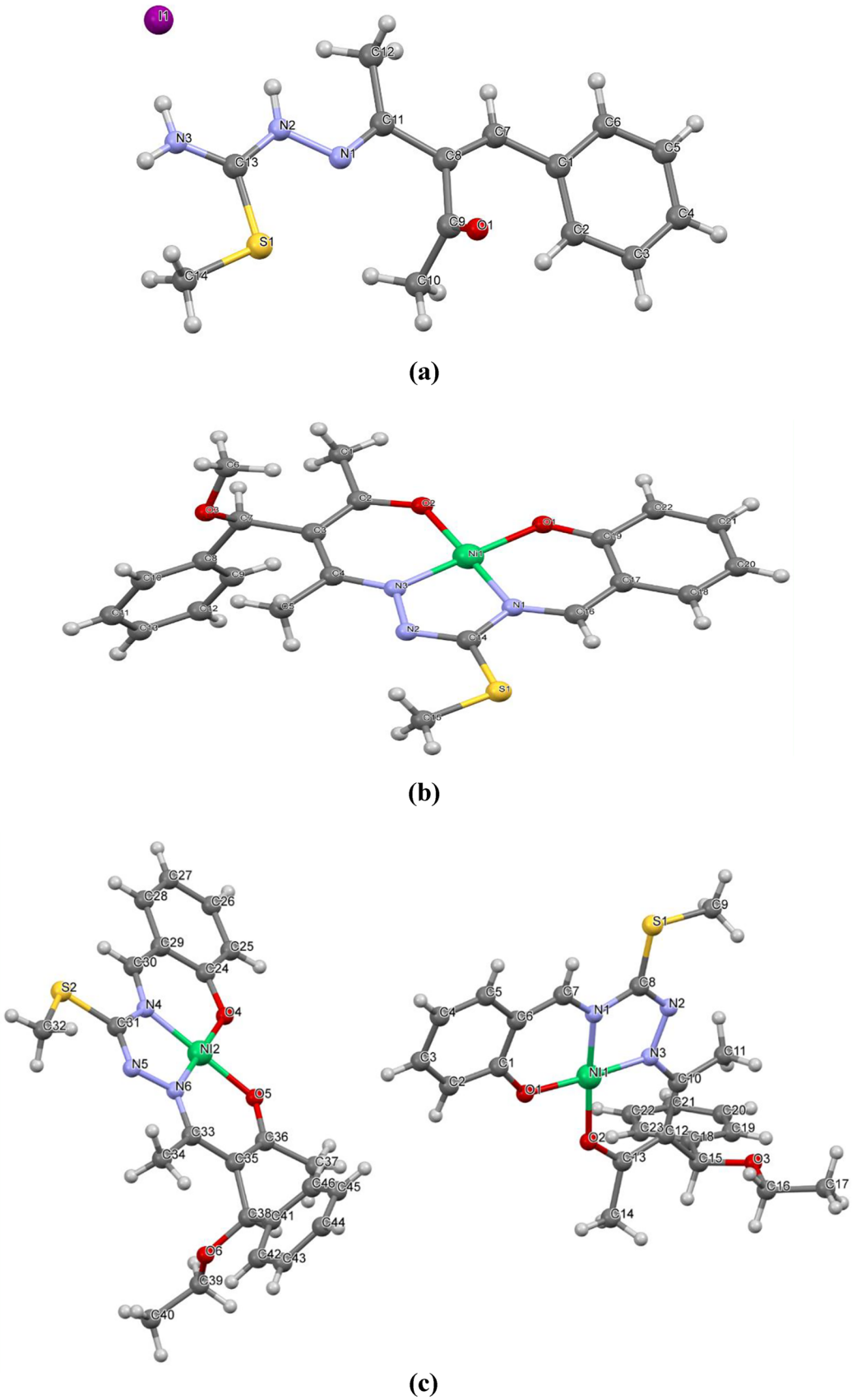

Fig. 3 The atomic numbering of TSC (**a**), Ni1 (**b**), and Ni2 (**c**) structures

Table 1 Crystal data and structure refinement parameters

	TSC	Ni1	Ni2
Empirical formula	$C_{14}H_{18}N_3OSI$	$C_{22}H_{23}N_3NiO_3S$	$C_{23}H_{25}N_3NiO_3S$
Formula weight	403.27	468.20	482.23
Crystal system	Monoclinic	Triclinic	Triclinic
Space group	*C2/c*	*P-1*	*P-1*
a (Å)	18.022 (10)	9.7554 (8)	8.875 (3)
b (Å)	8.816 (4)	10.1128 (8)	15.267 (5)
c (Å)	22.295 (10)	11.5913 (10)	17.511 (6)
α (°)	90.00	81.092 (2)	77.498 (12)
β (°)	110.54 (3)	88.587 (2)	88.911 (11)
γ (°)	90.00	71.105 (2)	74.622 (11)
V (Å^3)	3317 (3)	1068.47 (15)	2231.7 (13)
Z	8	2	4
D_c (g cm^{-3})	1.615	1.455	1.435
μ (mm^{-1})	2.06	1.03	0.99
θ range (°)	2.4–28.1	2.2–25.0	2.4–20.6
Measured refls	44,002	13,497	25,071
Independent refls	2961	3752	8127
R_{int}	0.044	0.061	0.091
S	1.21	1.08	1.23
R1/wR2	0.041/0.084	0.052/0.114	0.095/0.135
$\Delta\rho_{max}/\Delta\rho_{min}$ (eÅ^{-3})	0.51/-0.58	0.47/-0.29	0.48/-0.42

%), HOMO: C23(%18) + N51(%14) + Ni(%11) + S56(%10) + O54(%9) for Ni2. Finally, when the molecular potential map (MEP) (Fig. 5) calculated from the optimized molecular geometry of the TSC is examined, the regions encoded in red (most negative region) and blue (most positive region) are clearly seen. Looking at the MEP maps, the negative regions are on the O31 and N30 atoms, while the positive regions (blue) are on the hydrogen atoms. The MEP values on the O31 and N31 atoms on the MEP map are − 0.074 and − 0.065 a.u. (atomic unit), respectively. According to this result, it can be said that these two atoms are the most suitable regions in terms of electrophilic attack reaction, and in a complex structure to be formed with metal atoms, the most active regions will be the most active regions and the places where the metal atom will be bonded will be over these two atoms.

Hirshfeld surfaces

Hirshfeld surface analysis was carried out with Crystal Explorer [48] program to examine solid state behavior of compounds and intermolecular interactions. Hirshfeld surface (d_{norm}) is expressed by the following equation;

$$d_{norm} = \frac{d_{i-r_i^{vdw}}}{r_i^{vdw}} + \frac{d_{e-r_e^{vdw}}}{r_e^{vdw}}$$

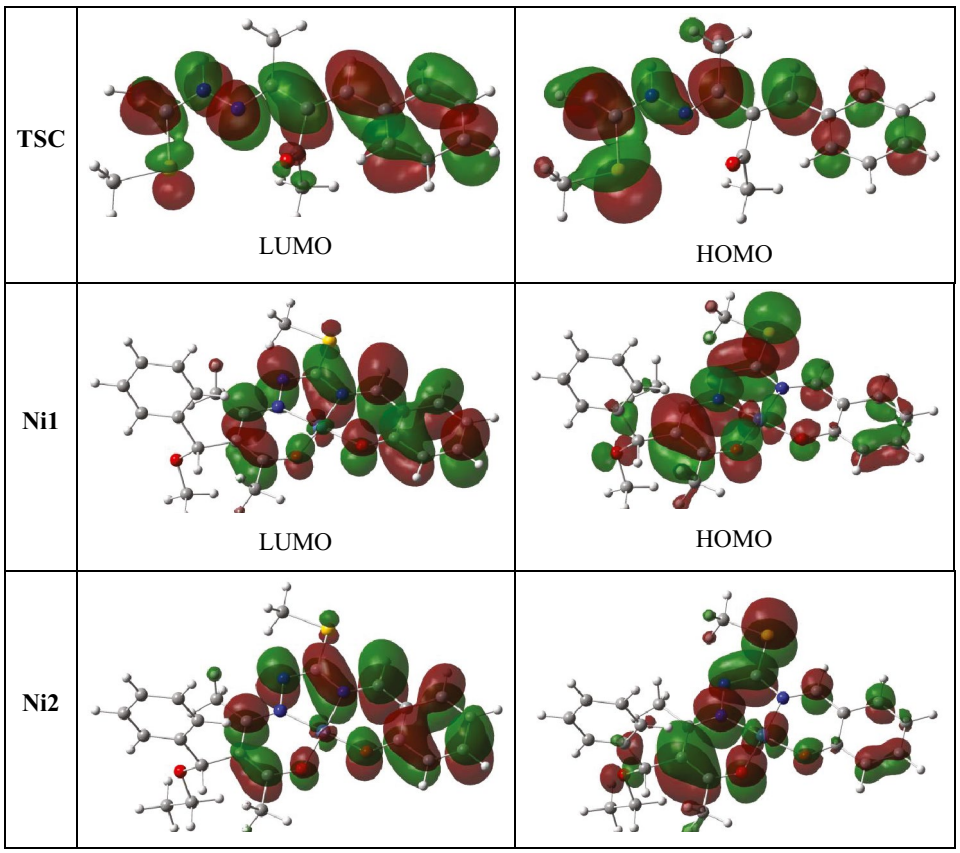

Fig. 4 Representation of HOMO–LUMO Frontier orbitals of TSC, Ni1, and Ni2

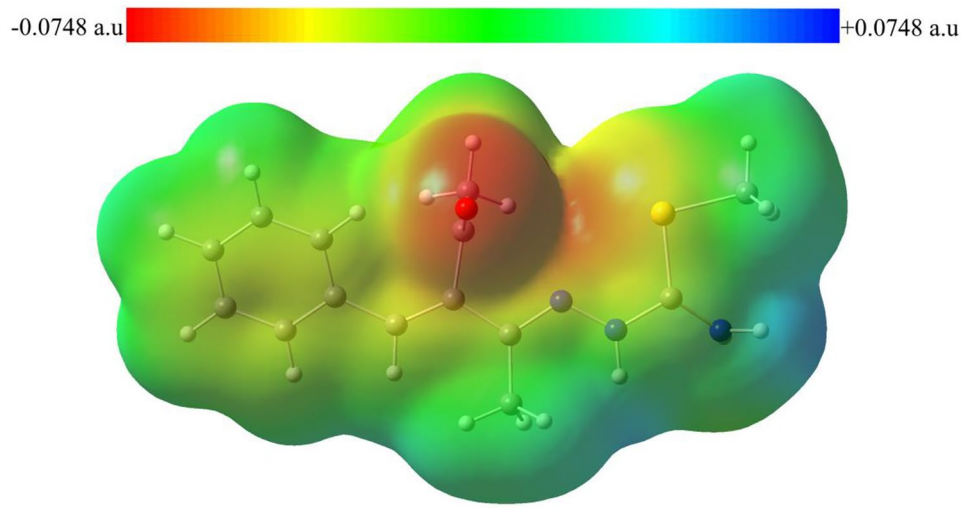

Fig. 5 MEP map derived from electron density of the TSC

In the equation, d_i and d_e are defined as the closest distances to the inner and outer atoms for points on the surface, respectively. The r_i^{vdw} and r_e^{vdw} represent van der Waals distances between atoms [49]. The curvedness and d_{norm} surfaces were determined to show the π-π and hydrogen bond interactions. Flat surfaces in the curvedness show the existence of π-π interactions in molecules [50]. Strong hydrogen bonds occur as a result of brief interatomic contacts, such as a dark red-stained surface on the d_{norm} [51]. The 2 dark red dots appearing on the dnorm surface in Fig. 6a represent strong C-H···O interactions. In Fig. 6b, the flat surface formed on the Cg1 ring of the Ni2 complex indicates that this ring can perform π-π interaction.

Antioxidant potential

The TEAC coefficients of the samples and that of standard ascorbic acid are shown in Table 2. It was revealed that the antioxidant capacity decreased in the order of TSC > ascorbic acid > Ni3 > Ni4 > Ni2 > Ni1.

The TEAC coefficient of TSC was close to ascorbic acid, but the lower values were obtained for the nickel complexes. The NH and keto groups in the thiosemicarbazone backbone must have contributed to the total antioxidant capacity [52–54].

The scavenging activity results showed that TSC (IC_{50}: 36.5 μM) showed lower activity as compared to ascorbic acid (IC_{50}: 8.8 μM). The nickel(II) complexes did not show any scavenging potency against DPPH radicals. This may be due to the nature of metal ion and its relative high redox potential [55]. In addition, it may be assumed that due to the steric hindrance of the larger chelate complex structure [56], the molecule cannot easily interact with the DPPH radical, and therefore the inactivity is observed. More importantly, radical scavenging potency is positively correlated with the number of hydroxyl groups in compounds [57]. It is known that the activity for some iron(III) and nickel(II) complexes was found to be much lower than the S-alkyl thiosemicarbazones due to the loss of the hydroxyl group after complex formation [24]. Additionally, considering the HOMO–LUMO gap values of 2.64 eV for TSC and about 3.08 eV for nickel complexes, it can be said that the reducing activity (= antioxidant performance) is limited due to the relatively high chemical hardness.

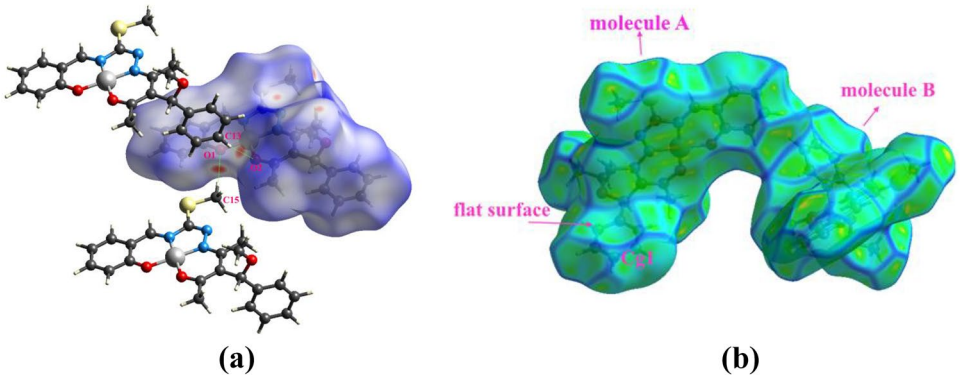

Fig. 6 **(a)** d_{norm} of Ni1 **(b)** curvedness surface of Ni2 with two crystallographically independent molecules (molecule A and molecule B)

Table 2 The TEAC coefficients of the compounds

Compounds	TEAC
TSC	1.18 ± 0.104
Ni1	0.44 ± 0.034
Ni2	0.47 ± 0.089
Ni3	0.57 ± 0.097
Ni4	0.49 ± 0.022
Ascorbic acid	1.02 ± 0.010

These results are in agreement with those of other studies. Hosseini-Yazdi et al. reported that a water soluble thiosemicarbazone ligand indicated higher radical scavenging relative to its nickel(II), copper(II) complexes, and ascorbic acid, and so the authors hypothesized that metal coordination decreases DPPH radical scavenging performance [58]. Another study showed that the bis-azo-Schiff base ligands exhibited higher scavenging activity than that of ascorbic acid, but its zinc(II) complexes did not have any activity [59].

Conclusions

The new nickel(II) complexes using the TSC as a starting material were characterized by experimental and theoretical methods. For the first time, we have shown that four n-alcohols (methyl, ethyl, propyl and allyl alcohols) are added to the C = C bond at the 2,4-pentanedione moiety via the Michael pathway and the alcohol provide a proton necessary to complete the chelate complex formation. Single-crystal XRD analysis displayed that the nickel(II) centers have distorted square planar environments. Antioxidant performances of the compounds were determined by means of DPPH and CUPRAC assays and the TSC showed higher activity compared to the self-derived nickel(II) complexes. DFT calculations yielded the FMO levels showing that the chemical hardness limits the antioxidant potential, as consistent with the experimental TEAC values.

Supplementary Information The online version contains supplementary material available at https://doi.org/10.1007/s11224-022-01908-0.

Acknowledgements The authors acknowledge to Scientific and Technological Research Application and Research Center, Sinop University, Turkey, for the use of the Bruker D8-QUEST diffractometer.

Author contributions Tuncay Karakurt: Formal analysis, methodology, data curation. Büşra Kaya: Investigation, writing—original draft. Onur Şahin: Investigation, formal analysis, data curation. Bahri Ülküseven: Project administration, supervision, witing—review and editing.

Funding This work was supported by the Scientific Research Projects Coordination Unit of Istanbul University-Cerrahpasa (Project numbers: 35177 and 34226).

Data availability All data generated or analyzed during this study are included in this published article [and its supplementary information files].

Code availability Not applicable.

Declarations

Conflict of interest The authors declare no competing interests.

References

1. Haribabu J, Srividya S, Mahendiran D et al (2020) Synthesis of Palladium(II) Complexes via Michael Addition: Antiproliferative Effects through ROS-Mediated Mitochondrial Apoptosis and Docking with SARS-CoV-2. Inorg Chem 59:17109–17122
2. Gutierrez E, Richardson DR, Jansson PJ (2014) The anticancer agent di-2-pyridylketone 4, 4-dimethyl-3-thiosemicarbazone (Dp44mT) overcomes prosurvival autophagy by two mechanisms: persistent induction of autophagosome synthesis and impairment of lysosomal integrity. J Biol Chem 289:33568–33589
3. Kunos CA, Sherertz TM (2014) Long-term disease control with triapine-based radiochemotherapy for patients with stage IB2–IIIB cervical cancer. Front Oncol 4:184
4. De Clercq E (2004) Antivirals and antiviral strategies. Nat Rev Microbiol 2:704–720
5. Falzon D, Hill G, Pal SN et al (2014) Pharmacovigilance and tuberculosis: applying the lessons of thioacetazone. Bull World Health Organ 92:918–919
6. Löber G, Hoffmann H (1990) Ambazone as a membrane active antitumor drug. Biophys Chem 35:287–300
7. Khan A, Jasinski JP, Smolenski VA et al (2018) Enhancement in anti-tubercular activity of indole based thiosemicarbazones on complexation with copper (I) and silver (I) halides: Structure elucidation, evaluation and molecular modelling. Bioorg Chem 80:303–318
8. Saswati, Mohanty M, Banerjee A et al (2020) Polynuclear zinc(II) complexes of thiosemicarbazone: Synthesis, X-ray structure and biological evaluation. J Inorganic Biochem 203:110908
9. Carcelli M, Tegoni M, Bartoli J et al (2020) In vitro and in vivo anticancer activity of tridentate thiosemicarbazone copper complexes: Unravelling an unexplored pharmacological target. European J Medicinal Chem 194:112266
10. Sharma D, Jasinski JP, Smolinski VA et al (2020) Synthesis and structure of complexes (NiII, AgI) of substituted benzaldehyde thiosemicarbazones and antitubercular activity of NiII complex. Inorganica Chimica Acta 499:119187
11. Matesanz AI, Leitao I, Souza P (2013) Palladium (II) and platinum (II) bis (thiosemicarbazone) complexes of the 2, 6-diacetylpyridine series with high cytotoxic activity in cisplatin resistant A2780cisR tumor cells and reduced toxicity. J Inorg Biochem 125:26–31
12. Matesanz AI, Hernández C, Souza P (2014) New bioactive 2, 6-diacetylpyridine bis (p-chlorophenylthiosemicarbazone) ligand and its Pd (II) and Pt (II) complexes: Synthesis, characterization, cytotoxic activity and DNA binding ability. J Inorg Biochem 138:16–23
13. Paterson BM, Donnelly PS (2011) Copper complexes of bis (thiosemicarbazones): from chemotherapeutics to diagnostic and therapeutic radiopharmaceuticals. Chem Soc Rev 40:3005–3018
14. Bal T, Atasever B, Solakoğlu Z et al (2007) Synthesis, characterisation and cytotoxic properties of the N1,

N4-diarylidene-S-methyl-thiosemicarbazone chelates with Fe(III) and Ni(II). Eur J Med Chem 42:161–167
15. Atasever B, Ülküseven B, Bal-Demirci T et al (2010) Cytotoxic activities of new iron(III) and nickel(II) chelates of some S-methyl-thiosemicarbazones on K562 and ECV304 cells. Invest New Drugs 28:421–432
16. Kaya B, Yılmaz ZK, Şahin O et al (2019) Structural analysis and biological functionalities of iron(III)– and manganese(III)–thiosemicarbazone complexes: in vitro anti-proliferative activity on human cancer cells, DNA binding and cleavage studies. J Biol Inorg Chem 24:365–376
17. Kaya B, Yılmaz ZK, Şahin O et al (2020) Structural characterization of new zinc(II) complexes with N2O2 chelating thiosemicarbazidato ligands; investigation of the relationship between their DNA interaction and in vitro antiproliferative activity towards human cancer cells. New J Chem 44:9313–9320
18. Özerkan D, Ertik O, Kaya B et al (2019) Novel palladium (II) complexes with tetradentate thiosemicarbazones. Synthesis, characterization, in vitro cytotoxicity and xanthine oxidase inhibition. Invest New Drugs 37:1187–1197
19. Kaya B, Atasever-Arslan B, Kalkan Z et al (2016) Apoptotic mechanisms of nickel(II) complex with N1-acetylacetone-N4-4-methoxy-salicylidene-S-allyl-thiosemicarbazone on HL60 leukemia Cells. Gen Physiol Biophys 35:451–458
20. Aruoma OI (1996) Assessment of potential prooxidant and antioxidant actions. J Am Oil Chem Soc 73:1617–1625
21. Raja DS, Paramaguru G, Bhuvanesh NSP et al (2011) Effect of terminal N-substitution in 2-oxo-1, 2-dihydroquinoline-3-carbaldehyde thiosemicarbazones on the mode of coordination, structure, interaction with protein, radical scavenging and cytotoxic activity of copper (II) complexes. Dalton Trans 40:4548–4559
22. Balakrishnan N, Haribabu J, Dhanabalan AK et al (2020) Thiosemicarbazone (s)-anchored water soluble mono-and bimetallic Cu (II) complexes: Enzyme-like activities, biomolecular interactions, anticancer property and real-time live cytotoxicity. Dalton Trans 49:9411–9424
23. Bal-Demirci T, Şahin M, Özyürek M et al (2014) Synthesis, antioxidant activities of the nickel(II), iron(III) and oxovanadium(IV) complexes with N2O2 chelating thiosemicarbazones. Spectrochim Acta A Mol Biomol Spectrosc 126:317–323
24. Kaya B, Şahin O, Bener M, Ülküseven B (2018) Iron(III) and nickel(II) complexes with S-alkyl (n-C1-6)- thiosemicarbazidato ligands: Synthesis, structural characterization, and antioxidant features. J Mol Struct 1167:16–22
25. Kaya B, Kaya K, Koca A, Ülküseven B (2019) Thiosemicarbazide-based iron(III) and manganese(III) complexes. Structural, electrochemical characterization and antioxidant activity. Polyhedron 173:114130
26. Haribabu J, Balachandran C, Tamizh MM et al (2020) Unprecedented formation of palladium (II)-pyrazole based thiourea from chromone thiosemicarbazone and [PdCl2 (PPh3) 2]: Interaction with biomolecules and apoptosis through mitochondrial signaling pathway. J inorganic biochem 205:110988
27. Sheldrick G (2008) A short history of SHELX. Acta Crystallographica Section A: Foundations and Advances A64:112–122
28. Sheldrick GM (2015) Crystal structure refinement with *SHELXL*. Acta Crystallographica Section C Structural Chemistry 71:3–8
29. Farrugia LJ (2012) WinGX and ORTEP for Windows: an update. J Appl Crystallogr 45:849–854
30. APEX2 (2013) APEX2. Bruker AXS Inc. Madison, Wisconsin, USA
31. Mercury, Version 3.3. CCDC, available online via http://www.ccdc.cam.ac.uk/products/mercury
32. Frish MJ, Trucks GW, Schlegel HB et al (2009) Gaussian 09, revision A. 02. Gaussian Inc, Wallingford CT
33. Becke AD (1993) Density-functional thermochemistry. III. The role of exact exchange. J Chem Phys 98:5648–5652
34. Lee C, Yang W, Parr RG (1988) Development of the Colle-Salvetti correlation-energy formula into a functional of the electron density. Phys Rev B 37:785
35. Hay PJ, Wadt WR (1985) Ab initio effective core potentials for molecular calculations. Potentials for the transition metal atoms Sc to Hg. J Chem Phys 82:270–283
36. Hay PJ, Wadt WR (1985) Ab initio effective core potentials for molecular calculations. Potentials for K to Au including the outermost core orbitals. J Chem Phys 82:299–310
37. Wadt WR, Hay PJ (1985) Ab initio effective core potentials for molecular calculations. Potentials for main group elements Na to Bi. J Chem Phys 82:284–298
38. Yamazaki C (1975) The Structure of Isothiosemicarbazones. Can J Chem 53:610–615
39. Leovac VM, Divjaković V, Češljević VI, Engel P (1987) Transition metal complexes with the thiosemicarbazide-based ligands-I. Nickel (II) complexes with the quadridentate ligands based on S-methylisothiosemicarbazide; X-ray crystal structure of (acetylacetone N(1)-salicylidene-S-methylizothiosemicarbazonato. Polyhedron 6:1901–1907
40. Kaya B, Koca A, Ülküseven B (2015) Asymmetric N2O2 complexes of iron(III) and nickel(II) obtained from acetylacetone-S-methyl-thiosemicarbazone: Synthesis, characterization and electrochemistry. J Coord Chem 68:586–598
41. Apak R, Güçlü K, Özyürek M, Karademir SE (2004) Novel total antioxidant capacity index for dietary polyphenols and vitamins C and E, using their cupric ion reducing capability in the presence of neocuproine: CUPRAC method. J Agric Food Chem 52:7970–7981
42. Sánchez-Moreno C, Larrauri JA, Saura-Calixto F (1998) A procedure to measure the antiradical efficiency of polyphenols. J Sci Food Agric 76:270–276
43. Kenichi F (1982) Role of Frontier Orbitals in Chemical Reactions. Science 218:747–754
44. Buyukuslu H, Akdogan M, Yildirim G, Parlak C (2010) Ab initio Hartree-Fock and density functional theory study on characterization of 3-(5-methylthiazol-2-yldiazenyl)-2-phenyl-1H-indole. Spectrochim Acta Part A Mol Biomol Spectrosc 75:1362–1369
45. Parr RG, Pearson RG (1983) Absolute hardness: companion parameter to absolute electronegativity. J Am Chem Soc 105:7512–7516
46. Parr RG, Donnelly RA, Levy M, Palke WE (1978) Electronegativity: The density functional viewpoint. J Chem Phys 68:3801–3807
47. Parr RG, Szentpály LV, Liu S (1999) Electrophilicity index. J Am Chem Soc 121:1922–1924
48. Spackman PR, Turner MJ, McKinnon JJ et al (2021) CrystalExplorer: a program for Hirshfeld surface analysis, visualization and quantitative analysis of molecular crystals. J Appl Crystallogr 54:1006–1011
49. Nami SAA, Sarikavakli N, Alam MJ et al (2017) Detailed molecular, structural and spectral studies of bimetallic salt,[Ni (L)][CoCl4] where L= 3, 7-bis (2-aminoethyl)-1, 3, 5, 7-tetraazabicyclo (3.3. 1) nonane. J Mol Struct 1138:90–101
50. Karakurt T, Cukurovali A, Kani İ (2020) Structure of 2-(2-(anthracen-9-ylmethylene) hydrazinyl)-4-(3-methyl-3-phenylcyclobutyl) thiazole by combined X-Ray crystallographic and molecular modelling studies. Molecular Physics 118:e1718224
51. Venkatesan P, Thamotharan S, Ilangovan A et al (2016) Crystal structure, Hirshfeld surfaces and DFT computation of NLO active (2E)-2-(ethoxycarbonyl)-3-[(1-methoxy-1-oxo-3-phenylpropan-2-yl) amino] prop-2-enoic acid. Spectrochim Acta Part A Mol Biomol Spectrosc 153:625–636
52. Nguyen DT, Le TH, Bui TTT (2013) Antioxidant activities of thiosemicarbazones from substituted benzaldehydes and

N-(tetra-O-acetyl-β-d-galactopyranosyl)thiosemicarbazide. Eur J Med Chem 60:199–207
53. Rice-Evans CA, Miller NJ, Paganga G (1996) Structure-antioxidant activity relationships of flavonoids and phenolic acids. Free Radical Biol Med 20:933–956
54. Gulcin İ (2020) Antioxidants and antioxidant methods: An updated overview. Arch Toxicol 94:651–715
55. Butkovic V, Klasinc L, Bors W (2004) Kinetic Study of Flavonoid Reactions with Stable Radicals. J Agric Food Chem 52:2816–2820
56. Xie J, Schaich KM (2014) Re-evaluation of the 2,2-diphenyl-1-picrylhydrazyl free radical (DPPH) assay for antioxidant activity. J Agric Food Chem 62:4251–4260
57. Mruthyunjayaswamy BHM (2017) Synthesis, spectroscopic characterization, electrochemistry and biological activity evaluation of some metal (II) complexes with ONO donor ligands containing indole and coumarin moieties. J Saudi Chem Soc 21:S202–S218
58. Hosseini-Yazdi SA, Mirzaahmadi A, Khandar AA et al (2017) Copper, nickel and zinc complexes of a new water-soluble thiosemicarbazone ligand: Synthesis, characterization, stability and biological evaluation. J Mol Liq 248:658–667
59. Özdemir Ö (2020) Bis-azo-linkage Schiff bases—Part(II): Synthesis, characterization, photoluminescence and DPPH radical scavenging properties of their novel luminescent mononuclear Zn(II) complexes. J Photochem Photobiol A: Chem 392:112356